Atmos. Chem. Phys. Discuss., 15, 13827–13865, 2015
www.atmos-chem-phys-discuss.net/15/13827/2015/
doi:10.5194/acpd-15-13827-2015

Atmospheric Chemistry and Physics Discussions

Influence of mineral dust and sea spray supermicron particle concentrations and acidity on inorganic NO_3^- aerosol during the 2013 Southern Oxidant and Aerosol Study

H. M. Allen[1,*], D. C. Draper[1,], B. R. Ayres[1], A. Ault[2,3], A. Bondy[2], S. Takahama[4], R. L. Modini[4], K. Baumann[5], E. Edgerton[5], C. Knote[6], A. Laskin[7], B. Wang[7], and J. L. Fry[1]**

[1]Department of Chemistry, Reed College, Portland, OR, USA
[2]Department of Chemistry, University of Michigan, Ann Arbor, MI, USA
[3]Department of Environmental Health Sciences, University of Michigan, Ann Arbor, MI, USA
[4]École Polytechnique Fèdèrale de Lausanne, Lausanne, Switzerland
[5]Atmospheric Research & Analysis, Inc., Cary, NC, USA
[6]Meteorologisches Institut, Ludwig-Maximilians-Universität, Munich, Germany
[7]William R. Wiley Environmental Molecular Sciences Laboratory, Pacific Northwest National Laboratory, Richland, Washington, USA

*now at: Division of Chemistry and Chemical Engineering, California Institute of Technology, Pasadena, CA, USA
**now at: Department of Chemistry, University of California, Irvine, CA, USA

Received: 28 February 2015 – Accepted: 24 April 2015 – Published: 13 May 2015

Correspondence to: J. L. Fry (fry@reed.edu)

Published by Copernicus Publications on behalf of the European Geosciences Union.

ACPD
15, 13827–13865, 2015

Abstract

The inorganic aerosol composition was measured in the southeastern United States, a region that exhibits high aerosol mass loading during the summer, as part of the 1 June to 15 July 2013 Southern Oxidant and Aerosol Study (SOAS) campaign. Measurements using a Monitor for AeRosols and GAses (MARGA), an ion chromatograph coupled with a wet rotating denuder and a steam-jet aerosol collector for monitoring of ambient inorganic gas and aerosol species, revealed two periods of high aerosol nitrate (NO_3^-) concentrations during the campaign. These periods of high nitrate were correlated with increased concentrations of coarse mode mineral or sea spray aerosol species, particularly Na^+ and Ca^{2+}, and with a shift towards aerosol with larger (1 to 2.5 µm) diameters. We suggest this nitrate aerosol forms by multiphase reactions of HNO_3 and particles, reactions that are facilitated by transport of mineral dust and sea spray aerosol from a source within the United States. The observed high aerosol acidity prevents the formation of NH_4NO_3, the inorganic nitrogen species often dominant in fine-mode aerosol at higher pH. Calculation of the rate of the heterogeneous uptake of HNO_3 on mineral aerosol supports the conclusion that aerosol NO_3^- is produced primarily by this process, and is likely limited by the availability of mineral dust surface area. Modeling of NO_3^- and HNO_3 by thermodynamic equilibrium models (ISORROPIA II and E-AIM) reveals the importance of including mineral cations in the southeastern United States to accurately balance ion species and predict gas/aerosol phase partitioning.

1 Introduction

Aerosol optical thickness measurements using remote sensing techniques indicate a high concentration of aerosol in the atmosphere over the southeastern United States during the summer months (Portmann et al., 2009). These aerosols likely arise from the significant concentrations of regional inorganic pollutants such as sulfur dioxide, and

ACPD
15, 13827–13865, 2015

from the oxidation of high concentrations of biogenic volatile organic compounds from regional vegetation (Goldstein et al., 2009). Anthropogenic NO_x (= NO and NO_2) acts as an important precursor in the oxidation of biogenic volatile organic compounds that leads to aerosol formation. Global emissions of NO_x and other anthropogenic nitrogen compounds have increased ten-fold in the last century and are expected to become a dominant pollutant in the near future as SO_2 concentrations decrease (Bauer et al., 2007; Doering et al., 2011), although NO_x concentrations are gradually decreasing in the southeast United States due to improved emission control technology (Russell et al., 2012). Thus, characterization of NO_x emissions and their relationship to aerosol formation can provide valuable constraints for atmospheric scientists seeking to understand the production of aerosol in the southeastern United States.

Aerosol NO_3^- forms in the atmosphere when NO_x, emitted from high-temperature combustion processes in vehicle engines and industrial facilities, reacts with OH radicals to form HNO_3 (Seinfeld and Pandis, 2006). This reaction is considered the dominant sink of daytime NO_x. Nighttime oxidation of NO_2 may form HNO_3 via a N_2O_5 intermediate (Jacob, 1999). In addition, NO_x can be oxidized in the aqueous phase following uptake into droplets or aqueous particles. After formation, HNO_3 dissociates in water droplets to produce aerosol NO_3^-. In the southeastern United States, NO_3^- typically comprises between 0.5 and 2 $\mu g\,m^{-3}$ of the annual 13 to 18 $\mu g\,m^{-3}$ total aerosol concentration (Blanchard and Hidy, 2003; Bauer et al., 2007). Yet HNO_3 is a semi-volatile species, and will readily partition between the gas and aerosol phases. As a result, the thermodynamic relationships governing aerosol NO_3^- concentrations are complex and highly dependent on the aerosol's chemical composition. Furthermore, aqueous-phase reactions may recycle HNO_3 back to the gas phase, further complicating the partitioning (Wang and Laskin, 2014).

In a polluted atmosphere, the anthropogenically emitted gas phase species NO_x, NH_3, and SO_2 serve as precursors for the formation of inorganic aqueous aerosol containing NO_3^-, NH_4^+, and SO_4^{2-}. Gaseous NH_3 will react with HNO_3 and H_2SO_4 to produce fine mode (< 1 µm diameter) NH_4NO_3 and various forms of ammoniated sul-

ACPD
15, 13827–13865, 2015

fates such as $(NH_4)_2SO_4$, $(NH_4)_3H(SO_4)_2$, and NH_4HSO_4, which are considered the dominant forms of these ions in the atmosphere (Finlayson-Pitts and Pitts, 2000; Seinfeld and Pandis, 2006; Baker and Scheff, 2007). However, the formation of NH_4NO_3 is typically limited by the amount of NH_4^+ available to neutralize both SO_4^{2-} and NO_3^- (Blanchard et al., 2000). In highly acidic environments, typically dominated by excess SO_4^-, the semi-volatile NH_4NO_3 will dissociate (Stelson and Seinfeld, 1982):

$$NH_4NO_{3(aq,s)} \rightleftharpoons NH_{3(g)} + HNO_{3(g)} \quad \text{(R1)}$$

Under these conditions, nitrate aerosol may still be formed when HNO_3 undergoes heterogeneous chemistry on the reactive surfaces of coarse mode (> 1 µm diameter) aerosol, such as sea spray and mineral dust, which act as reactive sinks toward HNO_3 (Dentener et al., 1996; Zhuang et al., 1999; Underwood et al., 2001; Yeatman et al., 2001; Lee et al., 2008). In sea salt (primarily NaCl) aerosol, HNO_3 displaces the Cl^- ion to form $NaNO_3$ and gas phase HCl, resulting in aerosol chloride depletion (Brimblecombe and Clegg, 1988; Zhuang et al., 1999):

$$NaCl_{(aq,s)} + HNO_{3(g)} \longrightarrow NaNO_{3(aq,s)} + HCl_{(g)} \quad \text{(R2)}$$

The multicomponent nature of sea spray means that analogous reactions may occur with other sea salt species, such as $MgCl_2$. Similarly, HNO_3 reacts with carbonates in mineral dust, such as $CaCO_3$ and $CaMg(CO_3)_2$, to form $Ca(NO_3)$ and $Mg(NO_3)_2$ (Laskin et al., 2005a; Gibson et al., 2006):

$$CaCO_{3(aq,s)} + 2HNO_{3(g)} \longrightarrow Ca(NO_3)_{2(aq,s)} + H_2O + CO_{2(g)} \quad \text{(R3)}$$

$$CaMg(CO_3)_{2(aq,s)} + 4HNO_{3(g)} \longrightarrow Ca(NO_3)_{2(aq,s)} + Mg(NO_3)_{2(aq,s)} + 2H_2O + 2CO_{2(g)} \quad \text{(R4)}$$

Sea spray and mineral dust have important implications for the total nitrogen budget, as these reactions facilitate a shift of NO_3^- from the fine mode to the coarse mode, and can enhance the amount of nitrate present in the aerosol. Globally, greater than 40 % of the total nitrate concentration is associated with mineral dust, and nearly all of the total nitrate may be coupled with coarse-mode mineral dust in regions exhibiting high

ACPD
15, 13827–13865, 2015

dust content (Usher et al., 2003). In addition, models of HNO_3 reactions on sea spray and mineral dust surfaces show that the equilibrium partitioning times are reached on the order of minutes, much faster than the deposition time of nitric acid in the air. As a result, more NO_3^- is retained in the aerosol phase at times of high sea spray and mineral dust concentrations and consequently, it is transported further than would otherwise occur in the atmosphere (Evans et al., 2004).

The present study seeks to understand the conditions under which inorganic nitrate aerosol formation occurs in the atmosphere in the southeastern United States. Measurements of inorganic aerosol and gas phase species were collected using ion chromatography, in an area of rural Alabama influenced by anthropogenic emissions. These measurements, coupled with airmass back trajectory analysis for source elucidation and with thermodynamic modeling, provide a glimpse into the fate of NO_x emissions and the formation of nitrate aerosol under conditions in which NH_4NO_3 formation is unfavored.

2 Experimental

2.1 Site description

The Southern Oxidant and Aerosol Study (SOAS) field campaign took place from 1 June to 15 July 2013 as part of a multi-institutional effort to understand biosphere–atmosphere interactions in the southeastern United States. The site chosen for this study was located in the United States Forest Service's National Talladega Forest near Centreville, Alabama (32.90289° N, 87.24968° W, and 126 m elevation). This site is part of the Southern Aerosol Research and Characterization network (SEARCH), which has been collecting data on EPA criteria gas and aerosol species since the early 1990s (http://www.atmospheric-research.com/studies/SEARCH/).

Due to its location in a heavily forested area, Centreville is primarily a rural site with high biogenic emissions from a mixture of conifer and deciduous trees. Proximity

ACPD
15, 13827–13865, 2015

to Birmingham, AL, located 71 km northeast of Centreville, causes the site to be influenced by elevated anthropogenic NO_x emissions. In addition, numerous coal-fired power plants in the region, including four within an 80 km radius, generate high point source SO_2 and NO_x emissions that raise concentrations of these pollutants when the wind direction transports those plumes to the site (see Fig. S1 in the Supplement).

2.2 Aerosol and gas composition

2.2.1 Bulk composition analysis via Monitor for AeRosols and GAses (MARGA)

Inorganic gas and aerosol composition at the SOAS site was characterized using a Monitor for AeRosols and GAses (MARGA) (Metrohm Applikon BV, Netherlands). The MARGA is a semi-continuous ion chromatography instrument designed to measure ambient concentrations of inorganic particulate matter (PM) and gases. Species detected by MARGA include gas phase HCl, HNO_3, HONO, NH_3, and SO_2, and particulate Cl^-, NO_3^-, SO_4^{2-}, NH_4^+, Na^+, K^+, Mg^{2+}, and Ca^{2+}. The MARGA inlet employs a wet rotating denuder (WRD) and a steam jet aerosol collector (SJAC), for collection of gases and particles respectively, in conjunction with cation and anion chromatography to report gas and aerosol concentrations at an hourly time resolution. The technique, including experimental detection limits, has been described in detail in Makkonen et al. (2012) and Rumsey et al. (2013). Table 1 presents a statistical summary of the MARGA measurements taken during the SOAS campaign.

At the SOAS ground site, ambient air was drawn through a PM_{10} (particles less than 10 µm in diameter) cyclone (Teflon coated, URG, Chapel Hill, NC), approximately 4 m a.g.l., at a flow rate of 16.7 standard liters per minute (sLpm). The sample air flowed through a 196 cm stretch of 2.70 cm inner diameter Teflon-coated aluminum at ambient temperature before reaching a $PM_{2.5}$ (particles less than 2.5 µm in diameter) cyclone (Teflon coated, URG, Chapel Hill NC). A further 147 cm length of 0.95 cm inner diameter polyethylene tubing at shelter temperature, giving a total inlet volume of 1224 cm^3 and a residence time of 4.4 s, brought the ambient air to the sample box. Once at

ACPD
15, 13827–13865, 2015

the sample box, the sample air passed through the WRD, in which absorption solution (10 ppm hydrogen peroxide, used as a biocide, in 18.2 MΩ deionized water) forms a thin aqueous film between two concentric rotating glass cylinders (Keuken et al., 1988). Water-soluble gasses diffuse into the absorbance solution while particles continue to the SJAC. The SJAC maintains a supersaturated environment with absorbance solution, in which particles activate and grow to micro-droplets and are then subsequently collected by inertial separation (Slanina et al., 2001).

Aqueous streams leading from the WRD and the SJAC accumulate for 60 min in separate 25 mL syringes. Once filled, the syringes inject the sample simultaneously with a 2.5 mL Li^+ and Br^- (320 and 3680 $\mu g L^{-1}$, respectively) internal standard into a 250 µL anion and a 500 µL cation injection loop before reaching the ion columns. A Metrosep C4 (100 × 4.0 mm) cation column, in conjunction with 3.2 mmol L^{-1} HNO_3 eluent and conductivity detector (Metrohm USA, Riverview, FL), separates and quantifies cationic species in the gas and the particle samples. Similarly, a Metrosep A Supp 10 (75 × 4.0 mm) column with Na_2CO_3–$NaHCO_3$ (7 and 8 mmol L^{-1} respectively) eluent and conductivity detector is used for detection of anions. During analysis, a second set of syringes acts in tandem configuration to collect sample for the next hour. HNO_3 is used to regenerate the suppressor ion exchange columns after analysis of each sample.

2.2.2 Single particle analysis via CCSEM and EDX

Samples for single particle analysis were collected using a multiple orifice uniform deposition impactor (MOUDI, MSP Corp. Model 110) sampling at 30 L min^{-1}. Particles were impacted on 200 mesh Carbon Type B with Formvar grids (Ted Pella Inc.) for analysis by computer-controlled scanning electron microscope (CCSEM) measurements with an FEI Quanta environmental dual focused ion beam scanning electron microscopy (FIB/SEM) equipped with a field emission gun operating at 20 kV and a high angle annular dark field (HAADF) detector (Laskin et al., 2002, 2006, 2012). The instrument was equipped with an energy dispersive X-ray (EDX) spectrometer (EDAX, Inc.)

ACPD
15, 13827–13865, 2015

which allows X-ray detection of elements with atomic numbers higher than Be. For the SOAS field campaign, 43 784 particles were analyzed. The CCSEM automated analysis captured single-particle physical properties including average diameter, projected area, and perimeter. EDX spectra from individual particles were also collected to determine the relative abundance of 22 elements: C, N, O, Na, Mg, Al, Si, P, S, Cl, Ag, K, Ca, Ti, V, Cr, Mn, Fe, Co, Ni, Zn, and Hg. Interferences from the TEM grid (C and O) and the HAADF detector (Si) were present. N could not be quantified due to interference from C, O, and the Bremsstrahlung background.

Single-particle analysis from the CCSEM-EDX was performed in MATLAB R2013b (Mathworks, Inc.) using k-means clustering of the elemental composition following the method previously described in Ault et al. (2012). Clusters were grouped into source-based classes by elemental composition, including mineral dust and sea spray aerosol (SSA). Mineral dust particles were characterized by high fractions and intensities of Al and Si, along with other crustal elements including Mg, Ca, K, Ti, and Fe (Sobanska et al., 2003; Krueger et al., 2004; Laskin et al., 2005b; Coz et al., 2009). Sea spray aerosol particles were characterized by the presence of Na and Mg in an approximately 10 : 1 ratio (Culkin and Cox, 1976; Pilson, 1998), which is the ratio of the two cations in seawater, along with K and Ca at appropriate ratios when detected during the 10–15 s EDX spectrum collection during CCSEM analysis. The fingerprint to identify SSA is based on laboratory and field studies of seawater generated SSA using SEM (Hopkins et al., 2008; Laskin et al., 2012; Ault et al., 2013b), including after reaction with HNO_3 (Liu et al., 2007; Ault et al., 2013a). Mineral dust was identified through fingerprints from previous studies, including Al, Si, and cation peaks (Na, Mg, K, and Ca) (Edgerton et al., 2009; Ault et al., 2012). Biomass was identified by C, O, K, and S (Posfai et al., 2003; Li et al., 2003; Edgerton et al., 2009; Moffet et al., 2010, 2013). SOA (secondary organic aerosol) was composed of different combinations of C, N, O, and S, which will be discussed further in a forthcoming publication with Raman microspectroscopy analysis (Moffet et al., 2010, 2013). Fly ash was determined through a combination of composition and shape analysis (Edgerton et al., 2009; Ault et al., 2012). Industrial

ACPD
15, 13827–13865, 2015

particles contained transition or heavier metals (Utsunomiya et al., 2004). Biological particles contained a mix of K, Ca, P, C (very high levels), and O (Edgerton et al., 2009; Huffman et al., 2012; Moffet et al., 2013). Soot was identified through composition (C and O), as well as morphology (Edgerton et al., 2009).

2.2.3 Elemental analysis via XRF

Elemental analysis of $PM_{2.5}$ collected on Teflon filters was performed via Energy Dispersive X-Ray Fluorescence (XRF) using a PANalytical (Westborough, MA) Epsilon-5 ED-XRF spectrometer. The Epsilon-5 was calibrated with MicroMatter (Vancouver, BC) XRF single element calibration standards, which are prepared by vacuum deposition on a polycarbonate substrate, resulting in a uniform deposit of the element with a nominal loading of $50 \pm 2.5\,\mu g\,cm^{-2}$. The results from the MicroMatter standards are then compared with the field samples containing $0.1–5\,\mu g\,cm^{-2}$ pollutant (Edgerton et al., 2005). The detection limits (LOD) were determined from field blank loadings assuming nominal sample volume of $24\,m^3$. Measurement precision was estimated from routine replicate analysis and from the average RSD of triplicate analyses from a sub-set of samples collected during the study. Accuracy was assessed using NIST-2783 (Air Particulate on Filter Media) and internally generated standards using a research-grade deposition chamber and verification protocol employing ICP-MS (Kul/ARA 0802A18 QCCHK) (Kulkarni, 2010).

2.2.4 Particle size via SMPS and APS

Particle size distributions were measured over the diameter range 0.01–20 µm with a Scanning Mobility Particle Sizer (SMPS 0.01–0.7 µm diameter; TSI Inc., Shoreview, MN, model 3080 consisting of a TSI model 3081 DMA and TSI model 3772 CPC), and an Aerodynamic Particle Sizer (APS 0.5–20 µm diameter; TSI model 3321). The instruments were operated outdoors in a ventilated tent to ensure that the temperature (and therefore relative humidity and particle size) was near ambient conditions. Verti-

ACPD
15, 13827–13865, 2015

cally oriented, stainless steel tubes (length 1.4 m, OD 0.25 in, ID 0.18 in) connected the SMPS inlet (flow rate 1 Lpm) and inner APS inlet (flow rate 1 Lpm) to a common, stainless steel inlet with purpose-build rain hat above the tent. A particle density of 1 g cm^{-3} and shape factor of 1 (corresponding to wet aerosols) were assumed for merging the SMPS and APS size distributions (Khlystov et al., 2004), and for calculating the integrated mass concentrations of PM_1 and $PM_{2.5}$.

2.2.5 Modeling via ISORROPIA and EAIM

ISORROPIA II, a thermodynamic equilibrium model for inorganic gases and aerosols in the atmosphere (available at http://isorropia.eas.gatech.edu) was employed to assess the equilibrium state of the aerosol found at Centreville, as well as to check the model's ability to accurately capture gas-aerosol chemistry in the atmosphere at Centreville. Concentrations of inorganic species measured with an hourly time resolution by MARGA were input into the model as total (gas + aerosol) concentrations: SO_4^{2-}, HNO_3+NO_3^-, NH_3+NH_4^+, Na^+, HCl+Cl^-, Ca^{2+}, K^+, and Mg^{2+}, along with temperature and relative humidity (RH) measurements. Temperature and RH measurements were collected at 1 min resolution from the Atmospheric Research and Analysis, Inc. (ARA) SEARCH monitoring site collocated with the SOAS ground site at Centreville, using a MET4 sensor probe (Paroscientific Inc, Redmond, WA) with 0.1 °C and 0.8 % accuracy for temperature and RH, respectively (Hansen et al., 2003). The meteorological data was averaged to hourly increments to match the time resolution of MARGA measurements input into the model. ISORROPIA II was run in the "forward" mode in the thermodynamically stable state, in which the model repartitions the gas and aerosol phase species assuming thermodynamic equilibrium conditions and salts precipitate once the aqueous phase becomes saturated, in order to determine if each species would be present in the gas, aerosol, or solid phases (Fountoukis and Nenes, 2007). E-AIM (Extended Aerosol Inorganics Model; available at http://www.aim.env.uea.ac.uk/aim/aim.php) model IV was similarly employed (inputs of total gas + aerosol concentrations of SO_4^{2-}, HNO_3+NO_3^-, NH_3+NH_4^+, Na^+, and

ACPD
15, 13827–13865, 2015

$HCl+Cl^-$, temperature, and RH with the model configured to allow salts to precipitate once the aqueous solution becomes saturated), but does not include the mineral species Ca^{2+}, K^+, and Mg^{2+} (Wexler and Clegg, 2007). E-AIM simulations require ion balance of all analytes, thus any cation deficiency was balanced using inputs of H^+. The sensitivity of the E-AIM model to variability in major analytes and to the ion balancing approach has been shown to be relatively minor (Young et al., 2013).

3 Results and discussion

3.1 Overview

During the SOAS campaign, HNO_3 and NO_3^- concentrations were relatively low compared to other inorganic ions such as sulfate and ammonium. Figure 1 presents the time series of HNO_3 and NO_3^- measurements between 1 June and 15 July 2013, along with subsets (Fig. 1b and c) indicating concentrations during periods of high NO_3^- concentrations. Gas phase HNO_3 concentrations averaged 0.34 $\mu g\,m^{-3}$ (0.14 ppb), with a maximum of 1.14 $\mu g\,m^{-3}$ (0.46 ppm) and a minimum of 0 $\mu g\,m^{-3}$ (0 ppm) (Table 1), and were typically highest during the early to late afternoon. The peak afternoon HNO_3 concentrations likely resulted from the increase in temperature that occurs between nighttime to daytime, which enhances nitrate partitioning to the gas phase as HNO_3. Aerosol NO_3^- exhibited an average concentration of 0.38 $\mu g\,m^{-3}$, encompassed a range from 0.03 to 1.07 $\mu g\,m^{-3}$ (Table 1), and typically peaked in the late morning to early afternoon. A separate collocated NO_3^- / HNO_3 measurement observed higher daytime concentrations of HNO_3, however, another measurement of HNO_3 via Chemical Ionization Mass Spectrometry at the site measured concentrations more similar to those reported by the MARGA. The observed range of [HNO_3] does not substantially affect the conclusions of this analysis (Sect. 3.5); see Supplement for comparison of these datasets. The higher daytime aerosol phase nitrate concentrations indicate most NO_3^-

ACPD
15, 13827–13865, 2015

is likely formed from the reaction of NO_2 via the daytime oxidant, OH. N_2O_5, which produces nighttime HNO_3 via hydrolysis, was measured at the field site, but due to slow N_2O_5 hydrolysis rates and high concentrations of organics in the surrounding area, likely contributed little to HNO_3 formation (Ayres et al., 2015). Periods of high NO_3^- concentrations ended as significant rainfall (3.5 mm of rain on 13 June and 1.9 mm on 28 June) removed aerosol from the air.

The high acidity of aerosol in the atmosphere of the southeastern United States during the summer would be expected to suppress aerosol NO_3^- formation, as high acidity is indicative of an atmosphere deficient in the cations necessary to partition nitrate into the aerosol phase. The correlation of SO_4^{2-} with NH_4^+ concentrations shows that the observed ammonium concentrations are insufficient to fully neutralize the existing sulfate (Fig. 2). Centreville is located in a region with numerous coal-fired power plants, leading to high concentrations of SO_4^{2-}, with an observed summertime range of 0.50 to 8.87 $\mu g\,m^{-3}$. Of the inorganic ions, SO_4^{2-} dominated the aerosol phase ionic composition and led to the highly acidic nature of the aerosol. The H^+ concentration was calculated by subtracting total charge equivalents of anions from that of cations in $\mu mol\,m^{-3}$:

$$[H^+] = \left[Cl^- + NO_3^- + 2 \times SO_4^{2-}\right] - \left[Na^+ + NH_4^+ + K^+ + 2 \times Mg^{2+} + 2 \times Ca^{2+}\right] \quad (1)$$

The average inferred H^+ concentration at the site was 8.44 $nmol\,m^{-3}$, with a range of 0.03 to 108.53 $nmol\,m^{-3}$, indicating a cation-deficiency and therefore highly acidic aerosol. However, the variable effects of liquid water, the buffering action of HSO_4^-/SO_4^{2-}, and the effect of species activity coefficients prevents an accurate measure of pH from the H^+ inferred by ion balance (Hennigan et al., 2015). The high acidity found in this study is in agreement with Guo et al. (2014), who report a mean pH of 0.94 ± 0.59 and a diurnal mean H^+ concentration between 0.5 and 2.5 $nmol\,m^{-3}$ at the SOAS ground site. This measured acidity is consistent with that of aerosol characterized as acidic in several other urban and non-urban studies (Koutrakis et al., 1988; Spengler et al., 1989; Brauer et al., 1991; Lee et al., 2008).

ACPD
15, 13827–13865, 2015

Modeling of the inorganic species by ISORROPIA II, which utilizes all inorganic species measured including minerals, produced an average predicted H^+ concentration of 0.32 nmol m^{-3} and a range of < 0.00 to 12.00 nmol m^{-3} of H^+, up to an order of magnitude lower than values inferred from MARGA measurements. The discrepancy between measured and modeled acidity likely arises from the difference between strong acidity (obtained by ion balance assuming full dissociation of acids as done with measurements above) and free acidity (obtained by calculating the extent of dissociation as provided by ISORROPIA II), as well as from differences in treatment of aerosol liquid water content and the H^+ activity coefficient, which ion balance does not take into account (Hennigan et al., 2015). Hydrogen ion concentrations calculated by ion balance are often higher than those estimated by models due to these differences (Saxena et al., 1993; Guo et al., 2014).

As a result of the high acidity, most ammonium at the site will be associated with sulfate in fine mode aerosol. The formation of fine mode aerosol NO_3^- is therefore limited by the availability of any NH_4^+ not already associated with sulfate, and nitrate will likely partition, given temperature and equilibria constraints, into the gas phase as HNO_3. The observed high ratio of gas phase HNO_3 to aerosol NO_3^- is consistent with these high acidity observations. However, as explored in the next section, NO_3^- aerosol was able to form in the coarse mode rather than fine mode due to the presence of other aerosol cation species.

3.2 Influence of mineral dust and sea spray on nitrate aerosol

Two periods occurred from 9–13 June (designated "coarse particle event 1") and 23–28 June 2013 (designated "coarse particle event 2"), in which unusually high aerosol NO_3^- was observed. These two events correspond with an increase in mineral species such as Na^+, Ca^{2+}, Mg^{2+}, and K^+, suggesting aerosol NO_3^- is primarily driven by the availability of these cations and resides in the coarse mode (Fig. 3). NO_3^- concentrations track with variations in the concentrations of these minerals, enough of which are

ACPD
15, 13827–13865, 2015

present to fully neutralize NO_3^- on a charge equivalent basis (Fig. 3c). The observed trends of aerosol Na^+ and Ca^{2+} support the conclusion that NO_3^- is predominately formed by displacement reactions of NaCl, $CaCO_3$, and other similar species. Early in the study, particularly around 9 and 10 June, relatively high concentrations of Cl^- were present with Na^+. Over a period of five days, Cl^- gradually diminished in the aerosol while NO_3^- concentrations increased (Fig. 3b). The reaction of HNO_3 on sea spray reaches equilibrium on the order of 5 to 20 min for particles between 1.0 and 3.2 µm in diameter (Evans et al., 2004), indicating that most coarse mode aerosol observed at the site had likely reached equilibrium. The decreased concentrations of Cl^- during the event thus suggest the reaction of HNO_3 and subsequent displacement of aerosol Cl^- with NO_3^- as the air mass aged.

Observations of aerosol size distribution during the first event also suggest the role of mineral dust in aerosol NO_3^- formation, as the high NO_3^- events corresponded to a shift in particle size towards aerosols with larger diameters (Fig. 3a). Between 9 and 13 June, aerosols with diameters in the 1–2.5 µm range (PM_1–$PM_{2.5}$) were more prevalent than those with diameters less than 1 µm (PM_1) (Fig. 3a). The increase towards higher diameter particles correspond to a similar increase in the concentrations of mineral dust species, such as Na^+ and Ca^{2+}, and of NO_3^-, suggesting that aerosol NO_3^- formation occurs as coarse mode $NaNO_3$ and $Ca(NO_3)_2$.

3.3 Mineral dust origin

The prominence of both Ca^{2+} and Na^+ suggest that the mixture of both reacted mineral dust and sea spray is important for aerosol NO_3^- formation, yet the two coarse particle events exhibited differences in their mineral composition. The first event appears to be more strongly influenced by sea spray transport, as Cl^- existed in significantly higher concentrations during this event than during any other time during the campaign. The first coarse particle event exhibited a higher percentage of Na^+ (12.0 %) than occurred during the second event (7.5 %), and the second event had no accompanying Cl^- as

ACPD
15, 13827–13865, 2015

indicated by Fig. 3. However, the low Mg^{2+} to Na^{+} molar ratio (0.08) during the first event relative to seawater (0.114) also suggests a non-sea-salt origin for at least some of the Na^{+} observed at this time (Jordan et al., 2015). The second event had a higher percent composition of the crustal elements Ca^{2+} (3.3 %) and Si (45.2 %) than was present during the first event (2.4 and 41.8 %, respectively) (Table 2), as well as a larger Ca^{2+} to Na^{+} ratio (0.302 for the first event and 0.509 for the second; for comparison, the Ca^{2+}/Na^{+} of seawater is 0.022 Jordan et al., 2015). The lack of observed Cl^{-} during the 23–28 June event may be due to a longer air mass transport that provided sufficient time for Cl^{-} depletion to occur before the air mass reached the sampling site. However, the high relative concentrations of Ca^{2+} and Si present during the second event could indicate that the differences in mineral composition are due to differences in the origin of the mineral dust or differing ratios of mineral dust and SSA between the two events, with a higher percentage of aerosol during the second event more likely originating from a continental rather than an ocean source.

Back trajectory analysis of the airmass origin during the two coarse particle events was conducted to elucidate the origin of the mineral species. The trajectories were computed using version 9.0 of the FLEXible PARTicle dispersion model (FLEXPART, Stohl et al., 1998, available at http://flexpart.eu/), driven by analysis of the Global Forecasting System (GFS) of the National Centers for Environmental Protection (NCEP). The calculations were conducted by randomly releasing 10 000 inert air parcels within a 3 h period from the location of the Centreville, AL site, and followed for three days. This resulted in time-resolved 3-D information on the location of the airmass prior to arrival at Centreville, AL, including uncertainty due to stochastic processes like convection or turbulence acting on the airmass. From this information, deterministic trajectories were calculated to better guide the reader. Selected results of the back trajectory analysis are presented in Fig. 4.

The wind back trajectory analysis shows similar wind patterns occurring during the two coarse particle events. At the beginning of both events, winds originated from the Gulf of Mexico and traveled north to reach the measurement side. As the events con-

ACPD
15, 13827–13865, 2015

tinued, wind patterns shifted and the air mass arrived from Texas traveling westwards along the continental United States until, near the end of each event, the air mass originated from a high elevation near the western coast of the United States. Although the overall pattern in wind trajectories is similar between the two coarse particle events, slight differences in the wind patterns at the beginning of each event may have contributed to the observed differences in composition of the aerosol. The air mass at the beginning of coarse particle event 1 travelled at low elevation (500–1000 m a.s.l.) across the Gulf of Mexico and continued at this elevation until reaching the site, thus likely collecting and transporting sea spray aerosol to Centreville (Fig. 4a). In contrast, the air mass from event 2 originated from the northern shore of the Gulf and traveled at a lower elevation over land (less than 500 m a.s.l.) and was over land for a greater period of time (Fig. 4c). Estimates of marine aerosol lifetimes suggest that the lifetime of these aerosol against deposition is on the order of 0.5 to 2 days (Jordan et al., 2015), indicating that any marine aerosol collected during the second event had likely undergone deposition from the air mass before reaching the SOAS site. These observations accord with the greater influence of marine aerosol on the first coarse particle event compared to the second (Fig. 3), and suggest a relatively local (within the United States) origin of the mineral dust aerosol.

3.4 Single-particle composition evidence for coarse-mode HNO_3 uptake

Individual particle analysis using CCSEM for the two coarse particle events was compared with the remainder of the campaign. Particle classes, determined from cluster analysis of EDX spectra, showed that the two coarse particle events contained a significantly higher percentage of mineral dust and sea spray aerosol, particularly in the supermicron size range, than was otherwise present during the course of the campaign (Fig. 5). During the two coarse particle events, between 15–20 % of particles analyzed with diameters smaller than 1 µm and between 30–50 % of particles with diameters larger than 1 µm consisted of mineral dust. By comparison, outside of these two events less than 5 % of fine mode particles analyzed and between 10–25 % of coarse mode

ACPD
15, 13827–13865, 2015

particles consisted of mineral dust. Averaged over all particle diameters, during the first coarse particle event (12 samples) 27 % of aerosols were mineral dust and 20 % were sea spray; while during the second coarse particle event (3 samples), 53 % of particles were mineral dust and 23 % were sea spray. These percentages are higher than those throughout the entire field study (5 June 2013 to 11 July 2013), in which 17 % of particles were mineral dust and 16 % were sea spray. As a result of the larger fraction of mineral dust and sea spray during these events, the relative fraction of secondary organic aerosol decreases from the majority (more than 50 %) of particles in the 1–2 µm range during non-coarse events to a significantly smaller fraction (approximately 25 %) of particles in the same diameter range during the coarse events.

SEM with EDX was also utilized to investigate the contribution of total nitrogen (including both inorganic and organic present, assuming minimal losses under the vacuum of the SEM) to particles collected during the campaign. The average weight percent of nitrogen per particle during the coarse particle events and non-coarse particle events varied as a function of particle diameter. Overall, a higher atomic weight percent of nitrogen was present in particles with diameters larger than 1 µm. In addition, the average number fraction of sea spray aerosol + mineral dust was similarly highest for coarse mode particles, increasing substantially for particles 1 µm or larger in diameter. The mixing of nitrate in sea spray aerosol will be described in detail in a forthcoming publication (Bondy et al., 2015). These data thus corroborate previous analysis on the impact of high acidity at the site by showing that very little nitrogen occurs in the fine mode in the aerosol and indicate the importance of mineral dust and sea spray aerosol in larger diameter particles.

3.5 Rate of nitrate production

In order to assess the contribution of mineral species to aerosol NO_3^- formation, the rate of the heterogeneous uptake of HNO_3 onto aerosol to form NO_3^- was determined using the Fuchs–Sutugin approach (Fuchs and Sutugin, 1971). This approach estimates the transition regime rate of uptake of HNO_3 onto measured aerosol surface area per unit

ACPD
15, 13827–13865, 2015

volume:

$$\text{rate} = \sum_{R_p} \frac{S_a}{R_p} D_g \left(\frac{0.75\alpha(1+Kn)}{Kn^2 + Kn + 0.283\alpha Kn + 0.75\alpha} \right) [HNO_3] \quad (2)$$

where S_a is the surface area per volume of aerosol in each size bin between 0.7 and 2.5 µm in diameter, R_p is the aerosol particle radius of the size bin, D_g is the diffusivity of HNO_3 in air ($0.118\,cm^2\,s^{-1}$, Durham and Stockburger, 1967), α is the accommodation coefficient, assumed to be the same as the kinetic regime measured uptake coefficient (γ, 0.1 for HNO_3, Usher et al., 2003), and Kn is the Knudsen number ($Kn = \frac{3D_g}{c_{HNO_3} R_p}$, $c_{HNO_3} = 341\,m\,s^{-1}$ at 298 K). Aerosol size distribution data were available only for the first of the two coarse particle events.

The rate of HNO_3 uptake necessitates the transition-regime approach because the aerosol size range assumed to be important for mineral dust or sea-salt uptake, 1–2.5 µm diameter, includes particles large enough to render the transition regime rate more appropriate than the commonly used kinetic uptake expression. A comparison of the rate predicted by Eq. (2) to the kinetic rate uptake expression (rate = $\frac{1}{4}\gamma_{HNO_3} S_a c_{HNO_3} [HNO_3]$) indicates that during peak coarse-mode loading on 13 June 2013, the transition-regime calculation is approximately 65 % of the rate derived from the kinetic expression.

The calculated rate of HNO_3 uptake onto aerosol surface area supports the conclusion that NO_3^- is produced primarily by this heterogeneous process. Figure 6 shows the calculated rate of production by heterogeneous uptake, along with factors that contribute to the rate of uptake such as $[HNO_3]$ and S_a. The average predicted rate of uptake during the campaign was approximately $0.07\,(\mu g\,m^{-3})\,h^{-1}$, but increased to higher than $0.50\,(\mu g\,m^{-3})\,h^{-1}$ during the first coarse particle event. This increase in rate of production was accompanied by a similar increase in the aerosol surface area of aerosol between 1 and 2.5 µm in diameter (Fig. 6c). Higher rates of aerosol NO_3^- production track more closely with higher S_a than with other factors that contribute to NO_3^-

ACPD
15, 13827–13865, 2015

formation, such as increased concentrations of gas phase HNO_3 (Fig. 6b). As a consequence, using alternate collocated HNO_3 measurements (see Supplement) does not affect the predicted aerosol NO_3^- production rates substantially. Thus, the limiting factor contributing to aerosol NO_3^- formation is likely the mineral dust surface area.

3.6 Modeling and measurement comparison

The results of the ISORROPIA II and E-AIM models and comparisons with measured values are presented in Fig. 7. The ISORROPIA II model predicted average nitrate chemistry relatively well, as the comparison between NO_3^- measured by MARGA and that predicted by ISORROPIA II shows a linear correlation (Fig. 7a), with a slope of 0.63 ± 0.06. However, ISORROPIA II both under- and over-predicted NO_3^- with respect to concentrations measured by MARGA, and the correlation produced a low R^2 value of 0.11. The deviations between model and measurement show a strong relationship with diurnal profile, and ISORROPIA II consistently under-predicted particulate NO_3^- concentrations during daylight hours but over-predicted them during the night, with the reverse for gas phase HNO_3 (Fig. 7b). The inflation of gas phase HNO_3 concentrations during the daytime shows a strong relationship with the diurnal profile of temperature, which similarly increases just after 6:00, peaks around 13:00–15:00, and gradually decreases to a low over the course of the night (Supplement). Predictions of NO_3^- using models like ISORROPIA II are often very sensitive to inputs of temperature, RH, and available ammonia (Markovic et al., 2011), and in the case of the southeastern United States, ISORROPIA II may contain a bias towards higher dependence on temperature for the volatile HNO_3 gas than was observed at Centreville, causing a stronger partitioning from aerosol to gas during times of high temperatures. As discussed in the Supplement, this discrepancy may also be due to an under-measurement of HNO_3 daytime peaks.

The importance of explicitly including mineral species in thermodynamic modeling is highlighted by the results from E-AIM. The model was unable to accurately assess

ACPD
15, 13827–13865, 2015

aerosol NO_3^- concentrations, consistently under-predicting concentrations of NO_3^- relative to measurements, and instead partitioning almost all available nitrate into the gas phase as HNO_3 (Fig. 7c and d). Correlations of modeled and measured aerosol NO_3^- produce an R^2 value of 2×10^{-4}. E-AIM, which includes only one mineral species (Na^+) in its thermodynamic calculations, manifests a strong dependence on RH, and does not predict any aerosol NO_3^- at RH < 90 %. Only during the nighttime, when RH values were higher, does E-AIM partition nitrate into the aerosol phase. The high temperatures and RH, combined with the acidic atmosphere in the southeastern United States and high presence of mineral aerosol species mean significant discrepancies may exist between observations and simulations when these mineral species are not considered in thermodynamic models. These findings are consistent with Trebs et al. (2005) and Metzger et al. (2006), who performed modeling studies of the Amazon and the Mediterranean, respectively, and with Karydis et al. (1988), all of whom similarly found that mineral cations must be explicitly included in inorganic models in order to obtain valid information on gas/aerosol partitioning and ionic balance.

4 Historical trends

Mineral dust and aerosol acidity have been shown to be important factors to consider when seeking to understand the chemistry that occurs in the atmosphere above the southeastern United States. The site chosen for this campaign is part of the SEARCH network, which has been continuously monitoring aerosol and gas composition at Centreville for the past five years and thus gives a historical record for assessing the importance of coarse mode nitrate in this area. Measurements of $PM_{2.5}$ aerosol species, such as NH_4^+, SO_4^{2-} and minerals, show that the site has a history of highly acidic aerosol and is often influenced by periodically high concentrations of sea spray and mineral dust aerosol. Annually averaged sulfate concentrations measured at the SEARCH site have exceeded ammonium concentrations by 8 to 20 % over the contin-

ACPD
15, 13827–13865, 2015

uous monitoring period 2008–2013 (see Fig. S2), showing that the high acidity measured during the SOAS campaign (Fig. 2) is typical of this site. Furthermore, the two coarse particle events appear to have frequent precedents. Over the five-year monitoring period, the site experienced 12–20 mineral dust events per year, and 20–42 sea spray events per year. Definitions of these events, annual totals, and full time series of mineral composition data averaged over three days are shown in the Supplement.

5 Conclusions

Gas and aerosol measurements of inorganic species in Centreville, AL indicate the importance of mineral dust and sea spray in the region. The southeastern United States is characterized by high emissions of SO_2, leading to high concentrations of aerosol SO_4^{2-}, which available NH_4^+ is insufficient to balance. As a result, the aerosol in this region is acidic and formation of the fine mode NH_4NO_3 is thermodynamically unfavorable. Instead, nitrate in the southeastern United States likely exists in the form of coarse mode NO_3^- balanced by the presence of mineral cations arising from transport of mineral dust and sea spray aerosol. Studies of aerosol composition and heterogeneous uptake rates of HNO_3 onto particle surfaces during the campaign indicate that NO_3^- is formed predominately from this pathway, with aerosol NO_3^- formation likely limited by the availability of mineral dust surfaces. Analysis of historical aerosol composition data collected at this site also shows acidity and mineral dust levels similar to those found during the summer 2013 SOAS campaign, indicating the long-term importance of acidity and mineral dust and the need for consideration of this coarse particle mediated heterogeneous loss process for NO_x during assessments of the chemistry of the atmosphere, particularly in the southeastern United States.

The Supplement related to this article is available online at doi:10.5194/acpd-15-13827-2015-supplement.

ACPD
15, 13827–13865, 2015

Acknowledgements. The authors would like to thank Annmarie Carlton, Jose-Luis Jimenez, and everyone who helped organize the SOAS field campaign. We would also like to thank Metrohm Applikon for use of the MARGA instrument, and in particular J. T. Stanton for invaluable instrument troubleshooting advice. Chuck Brock, Greg Frost, and Stu McKeen provided a useful NEI emissions mapping tool that aided our analysis. Tran Nguyen, Alex Teng, John Crounse, Jason St. Clair, and Paul Wennberg provided very useful HNO_3 data from their CIMS instrument. We acknowledge support from EPA-STAR RD-83539901 and the Reed College Mellon Environmental Studies Summer Experience Fellowship. Funding for single particle analysis was provided by EPA (R835409). CCSEM was performed at the Environmental Molecular Sciences Laboratory (EMSL), a national scientific user facility located at the Pacific Northwest National Laboratory (PNNL) and sponsored by the Office of Biological and Environmental Research of the U.S. Department of Energy (DOE). PNNL is operated for DOE by Battelle Memorial Institute under Contract No. DE-AC06-76RL0 1830. Travel funds to PNNL were provided by the University of Michigan Rackham Graduate School. Steve Bertman, Paul Shepson, Manelisi Nhliziyo, and Kerri Pratt assisted with funding, logistics, and sampling at SOAS for the single particle analysis.

References

Ault, A. P., Peters, T. M., Sawvel, E. J., Casuccio, G. S., Willis, R. D., Norris, G. A., and Grassian, V. H.: Single-particle SEM-EDX analysis of iron-containing coarse particulate matter in an urban environment: sources and distribution of iron within Cleveland, Ohio, Environ. Sci. Technol., 46, 4331–4339, 2012. 13835

Ault, A. P., Guasco, T. L., Ryder, O. S., Baltrusaitis, J. Cuadra-Rodriguez, L. A., Collins, D. B., Ruppel, M. J., Bertram, T. H., Prather, K. A., and Grassian, V. H.: Inside versus outside: ion redistribution in nitric acid reacted sea spray aerosol particles as determined by single-particle analysis, J. Am. Chem. Soc., 135, 14528–14531, 2013a. 13835

Ault, A. P., Moffet, R. C., Baltrusaitis, J., Collins, D. B., Ruppel, M. J., Cuadra-Rodriguez, L. A., Zhao, D., Guasco, T. L., Ebben, C. J., Geiger, F. M., Bertram, T. H., Prather, K. A., and Grassian, V. H.: Size-dependent changes in sea spray aerosol composition and properties with different seawater conditions, Environ. Sci. Technol., 47, 5603–5612, 2013b. 13835

ACPD
15, 13827–13865, 2015

Ayres, B. R., Allen, H. M., Draper, D. C., Brown, S. S., Jimenez, J. L., Day, D. A., De Gouw, J., Cohen, R. C., Baumann, K., Takahama, S., Thornton, J. A., Goldstein, A. H., and Fry, J. L.: NO_y fate at SOAS 2013: organonitrate formation via NO_3 + BVOC and inorganic nitrate formation via heterogeneous uptake of HNO_3, in preparation, 2015. 13839

Baker, K. and Scheff, P.: Photochemical model performance for PM2.5 sulfate, nitrate, ammonium, and precursor species SO_2, HNO_3, and NH_3 at background monitor locations in the central and eastern United States, Atmos. Environ., 41, 6185–6195, 2007. 13831

Bauer, S. E., Koch, D., Unger, N., Metzger, S. M., Shindell, D. T., and Streets, D. G.: Nitrate aerosols today and in 2030: a global simulation including aerosols and tropospheric ozone, Atmos. Chem. Phys., 7, 5043–5059, doi:10.5194/acp-7-5043-2007, 2007. 13830

Blanchard, C. and Hidy, G.: Effects of changes in sulfate, ammonia, and nitric acid on particulate nitrate concentrations in the southeastern United States, JAPCA J. Air Waste Ma., 53, 283–290, 2003. 13830

Blanchard, C. L., Roth, P. M., and Tanenbaum, S. J.: The use of ambient measurements to identify which precursor species limit aerosol nitrate formation, JAPCA J. Air Waste Ma., 50, 2073–2084, 2000. 13831

Bondy, A. L., Craig, R. L., Wang, B., Laskin, A., Nhliziyo, M. V., Bertman, S. B., Shepson, P. B., Pratt, K. A., and Ault, A. P.: Varying reactivity of sea spray aerosol measured at an inland sampling site during the Southern Oxidant and Aerosol Study (SOAS), in preparation, 2015. 13844

Brauer, M., Koutrakis, P., Keeler, G., and Spengler, J.: Indoor and outdoor concentrations of inorganic acidic aerosols and gases, JAPCA J. Air Waste Ma., 41, 171–181, 1991. 13839

Brimblecombe, P. and Clegg, S.: The solubility and behavior of acidic gases in the marine aerosol, J. Atmos. Chem., 7, 1–18, 1988. 13831

Coz, E., Gómez-Moreno, F. J., Pujada, M., Casuccio, G. S., Lersch, T. L., and Artiñano, B.: Individual particle characteristics of North African dust under different long-range transport scenarios, Atmos. Environ., 43, 1850–1863, 2009. 13835

Culkin, F. and Cox, R. A.: Sodium, potassium, magnesium, calcium, and strontium in sea water, Deep-Sea Res. Ocean. Abstr., 13, 789–804, 1976. 13835

Dentener, F. J., Carmichael, G. R., Zhang, Y., Lelieveld, J., and Crutzen, P. J.: Role of mineral aerosol as a reactive surface in the global troposphere, J. Geophys. Res.-Atmos., 101, 22869–22889, 1996. 13831

ACPD
15, 13827–13865, 2015

Doering, O., Galloway, T., and Swackhamer, D.: Reactive Nitrogen in the United States: an analysis of inputs, flows, consequences, and management options, United States Environmental Protection Agency, 2011. 13830
Durham, J. L. and Stockburger, L.: Nitric acid-air diffusion coefficient: experimental determination, Atmos. Environ., 20, 559–563, 1967. 13845
Edgerton, E., Hartsell, B., Saylor, R., Jansen, J., Hansen, D., and Hidy, G.: The Southeastern Aerosol Research and Characterization study: Part II. Filter-based measurements of fine and coarse particulate matter mass and composition, J. Air Waste Manage., 10, 1527–1542, 2005. 13836
Edgerton, E., Casuccio, G., Saylor, R. D., Lersch, T. L., Hartsell, B. E., Jansen, J. J., and Hansen, D. A.: Measurements of OC and EC in coarse particulate matter in the southeastern United States, J. Geophys. Res.-Atmos., 59, 78–90, 2009. 13835, 13836
Evans, M. C., Campbell, S. W., Bhethanabotla, V., and Poor, N. D.: Effect of sea salt and calcium carbonate interactions with nitric acid on the direct dry deposition of nitrogen to Tampa Bay, Florida, Atmos. Environ., 38, 4847–4858, 2004. 13832, 13841
Finlayson-Pitts, B. J. and Pitts, J. N.: Chemistry of the Upper and Lower Atmosphere: Theory, Experiments, and Applications, Academic Press, San Diego, CA, 2000. 13831
Fountoukis, C. and Nenes, A.: ISORROPIA II: a computationally efficient thermodynamic equilibrium model for K^+–Ca^{2+}–Mg^{2+}–NH_4^+–Na^+–SO_4^{2-}–NO_3^-–Cl^-–H_2O aerosols, Atmos. Chem. Phys., 7, 4639–4659, doi:10.5194/acp-7-4639-2007, 2007. 13837
Fuchs, N. A. and Sutugin, A. G.: High dispersed aerosols, in: Topics in Current Aerosol Research (Part 2), edited by: Hidy, G. M. and Brock, J. R., Pergamon, New York, 2541–2548, 1971. 13844
Gibson, E., Hudson, P., and Grassian, V.: Physicochemical properties of nitrate aerosols: implications for the atmosphere, J. Phys. Chem. A, 110, 11785–11799, 2006. 13831
Goldstein, A., Koven, C., Heald, C., and Fung, I.: Biogenic carbon and anthropogenic pollutants combine to form a cooling haze over the southeastern United States, P. Natl. Acad. Sci. USA, 106, 8835–8840, 2009. 13830
Guo, H., Xu, L., Bougiatioti, A., Cerully, K. M., Capps, S. L., Hite, J. R., Carlton, A. G., Lee, S.-H., Bergin, M. H., Ng, N. L., Nenes, A., and Weber, R. J.: Particle water and pH in the southeastern United States, Atmos. Chem. Phys. Discuss., 14, 27143–27193, doi:10.5194/acpd-14-27143-2014, 2014. 13839, 13840

ACPD
15, 13827–13865, 2015

Hansen, D. A., Edgerton, E. S., Hartsell, B. E., Jansen, J. J., Kandasamy, N., Hidy, G. M., and Blanchard, C. L.: The Southern Aerosol Research and Characterization study: Part 1 – Overview, J. Air Waste Manage., 53, 1460–1471, 2003. 13837

Hennigan, C. J., Izumi, J., Sullivan, A. P., Weber, R. J., and Nenes, A.: A critical evaluation of proxy methods used to estimate the acidity of atmospheric particles, Atmos. Chem. Phys., 15, 2775–2790, doi:10.5194/acp-15-2775-2015, 2015. 13839, 13840

Hopkins, R. J., Desyaterik, Y., Tivanski, A. V., Zaveri, R. A., Berkowitz, C. M., Tyliszczak, T., Gilles, M. K., and Laskin, A.: Chemical speciation of sulfur in marine cloud droplets and particles: analysis of individual particles from the marine boundary layer over the California current, J. Geophys. Res.-Atmos., 113, D008954, doi:10.1029/2007JD008954, 2008. 13835

Huffman, J. A., Sinha, B., Garland, R. M., Snee-Pollmann, A., Gunthe, S. S., Artaxo, P., Martin, S. T., Andreae, M. O., and Pöschl, U.: Size distributions and temporal variations of biological aerosol particles in the Amazon rainforest characterized by microscopy and real-time UV-APS fluorescence techniques during AMAZE-08, Atmos. Chem. Phys., 12, 11997–12019, doi:10.5194/acp-12-11997-2012, 2012. 13836

Jacob, D. J.: Introduction to Atmospheric Chemistry, Princeton University Press, Princeton, NJ, 1999. 13830

Jordan, C. E., Pszenny, A. A. P., Keene, W. C., Cooper, O. R., Deegan, B., Maben, J. R., Routhier, M., Sander, R., and Young, A. H.: Origins of aerosol chlorine during winter over north central Colorado, USA, J. Geophys. Res., 120, 678–694, 2015. 13842, 13843

Karydis, V. A., Tsimpidi, A. P., Fountoukis, C., Nenes, A., Zavala, M., Lei, W., Molina, L. T., and Pandis, S. N.: Simulating the fine and coarse inorganic particulate matter concentrations in a polluted megacity, Atmos. Environ., 44, 608–620, 1988. 13847

Keuken, M. P., Schoonebeek, C. A. M., van Wensveen-Louter, A., and Slanina, J.: Simultaneous sampling of NH_3, HNO_3, HCl, SO_2 and H_2O_2 in ambient air by a wet annular denuder system, Atmos. Environ., 22, 2541–2548, 1988. 13834

Khlystov, A., Stanier, C., and Pandis, S. N.: An algorithm for combining electrical mobility and aerodynamic size distributions data when measuring ambient aerosol, Aerosol Sci. Tech., 38, 229–238, 2004. 13837

Koutrakis, P., Wolfson, J., and Spengler, J.: An improved method for measuring aerosol strong acidity: results from a nine-month study in St. Louis, Missouri and Kingston, Tennessee, Atmos. Environ., 22, 157–162, 1988. 13839

ACPD
15, 13827–13865, 2015

Krueger, B. J., Grassian, V. H., Cowin, J. P., and Laskin, A.: Heterogeneous chemistry of individual mineral dust particles from different dust source regions: the importance of particle mineralogy, Atmos. Environ., 38, 6253–6261, 2004. 13835

Kulkarni, S.: Calibration and check samples for ED-XRF and WD-XRF, brochure, KulTech Incorporated, 311 S. Academy Street, Cary, NC 27511, 2010. 13836

Laskin, A., Idedema, M. J., and Cowin, J. P.: Quantitative time-resolved monitoring of nitrate formation in sea salt particles using a CCSEM/EDX single particle analysis, Environ. Sci. Technol., 36, 4948–4955, 2002. 13834

Laskin, A., Iedema, M. J., Ichkovich, A., Graber, E. R., Taraniuk, I., and Rudich, Y.: Direct observation of completely processed calcium carbonate dust particles, Faraday Discuss., 130, 453–468, 2005a. 13831

Laskin, A., Wietsma, T. W., Krueger, B. J., and Grassian, V. H.: Heterogeneous chemistry of individual mineral dust particles with nitric acid: a combined CCSEM/EDX, ESEM, and ICP-MS study, J. Geophys. Res.-Atmos., 110, D10208, doi:10.1029/2004JD005206, 2005b. 13835

Laskin, A., Cowin, J. P., and Iedema, M. J.: Analysis of individual environmental particles using modern methods of electron microscopy and X-ray microanalysis, J. Electron Spectrosc., 150, 260–274, 2006. 13834

Laskin, A., Moffet, R. C., Gilles, M. K., Fast, J. D., Zaveri, R. A., Wang, B. B., Nigge, P., and Shutthanandan, J.: Tropospheric chemistry of internally mixed sea salt and organic particles: surprising reactivity of NaCl with weak organic acids, J. Geophys. Res.-Atmos., 117, D017743, doi:10.1029/2012JD017743, 2012. 13834, 13835

Lee, T., Yu, X., Ayres, B., Kreidenweis, S. M., Malm, W. C., and Collett, J. L.: Observations of fine and coarse particle nitrate at several rural locations in the United States, Atmos. Environ., 42, 2720–2732, 2008. 13831, 13839

Li, J., Posfai, M., Hobbs, P. V., and Buseck, P. R.: Individual aerosol particles from biomass burning in southern Africa: 2. Compositions and aging of inorganic particles, J. Geophys. Res.-Atmos., 108, 8484, doi:10.1029/2002JD002310, 2003. 13835

Liu, Y., Cain, J. P., Wang, H., and Laskin, A.: Kinetic study of heterogeneous reaction of deliquesced NaCl particles with gaseous HNO_3 using particle-on-substrate stagnation flow reactor approach, J. Phys. Chem. A, 111, 10026–10042, 2007. 13835

Makkonen, U., Virkkula, A., Mäntykenttä, J., Hakola, H., Keronen, P., Vakkari, V., and Aalto, P. P.: Semi-continuous gas and inorganic aerosol measurements at a Finnish urban site: compar-

ACPD
15, 13827–13865, 2015

isons with filters, nitrogen in aerosol and gas phases, and aerosol acidity, Atmos. Chem. Phys., 12, 5617–5631, doi:10.5194/acp-12-5617-2012, 2012. 13833, 13857
Markovic, M. Z., Hayden, K. L., Murphy, J. G., Makar, P. A., Ellis, R. A., Chang, R. Y.-W., Slowik, J. G., Mihele, C., and Brook, J.: The effect of meteorological and chemical factors on the agreement between observations and predictions of fine aerosol composition in south-western Ontario during BAQS-Met, Atmos. Chem. Phys., 11, 3195–3210, doi:10.5194/acp-11-3195-2011, 2011. 13846
Metzger, S., Mihalopoulos, N., and Lelieveld, J.: Importance of mineral cations and organics in gas-aerosol partitioning of reactive nitrogen compounds: case study based on MINOS results, Atmos. Chem. Phys., 6, 2549–2567, doi:10.5194/acp-6-2549-2006, 2006. 13847
Moffet, R. C., Henn, T. R., Tivanski, A. V., Hopkins, R. J., Desyaterik, Y., Kilcoyne, A. L. D., Tyliszczak, T., Fast, J., Barnard, J., Shutthanandan, V., Cliff, S. S., Perry, K. D., Laskin, A., and Gilles, M. K.: Microscopic characterization of carbonaceous aerosol particle aging in the outflow from Mexico City, Atmos. Chem. Phys., 10, 961–976, doi:10.5194/acp-10-961-2010, 2010. 13835
Moffet, R. C., Rödel, T. C., Kelly, S. T., Yu, X. Y., Carroll, G. T., Fast, J., Zaveri, R. A., Laskin, A., and Gilles, M. K.: Spectro-microscopic measurements of carbonaceous aerosol aging in Central California, Atmos. Chem. Phys., 13, 10445–10459, doi:10.5194/acp-13-10445-2013, 2013. 13835, 13836
Pilson, M. E. Q.: An Introduction to the Chemistry of the Sea, Prentice Hall, New York, 1998. 13835
Portmann, R., Solomon, S., and Hegerl, G.: Spatial and season patterns in climate change, temperatures, and precipitation across the United States, P. Natl. Acad. Sci. USA, 106, 7324–7329, 2009. 13829
Posfai, M., Simonics, R., Li, J., Hobbs, P. V., and Buseck, P. R.: Individual aerosol particles from biomass burning in southern Africa: 1. Compositions and size distributions of carbonaceous particles, J. Geophys. Res.-Atmos., 108, 8483, doi:10.1029/2002JD002291, 2003. 13835
Rumsey, I. C., Cowen, K. A., Walker, J. T., Kelly, T. J., Hanft, E. A., Mishoe, K., Rogers, C., Proost, R., Beachley, G. M., Lear, G., Frelink, T., and Otjes, R. P.: An assessment of the performance of the Monitor for AeRosols and GAses in ambient air (MARGA): a semi-continuous method for soluble compounds, Atmos. Chem. Phys., 14, 5639–5658, doi:10.5194/acp-14-5639-2014, 2014. 13833

ACPD
15, 13827–13865, 2015

Russell, A. R., Valin, L. C., and Cohen, R. C.: Trends in OMI NO_2 observations over the United States: effects of emission control technology and the economic recession, Atmos. Chem. Phys., 12, 12197–12209, doi:10.5194/acp-12-12197-2012, 2012. 13830

Saxena, P., Mueller, P. K., Kim, Y. P., Seinfeld, J. H., and Koutrakis, P.: Coupling thermodynamic theory with measurements to characterize acidity of atmospheric particles, Aerosol Sci. Tech., 19, 279–293, 1993. 13840

Seinfeld, J. H. and Pandis, S. N.: Atmospheric Chemistry and Physics: from Air Pollution to Climate Change, 2nd edn., John Wiley & Sons, New York, 2006. 13830, 13831

Slanina, J., ten Brink, H., Otjes, R., Even, A., Jongejan, P., Khlystov, A., Waijers-Ijpelaan, A., Hu, M., and Lu, Y.: The continuous analysis of nitrate and ammonium in aerosols by the steam jet aerosol collector (SJAC): extension and validation of the methodology, Atmos. Environ., 35, 2319–2330, 2001. 13834

Sobanska, S., Coeur, C., Maenhaut, W., and Adams, F.: SEM-EDX characterization of tropospheric aerosols in the Nagev desert (Israel), J. Atmos. Chem., 44, 299–322, 2003. 13835

Spengler, J., Keeler, G., Koutrakis, P., Ryan, P., Raisenne, M., and Franklin, C.: Exposures to acidic aerosol, Environ. Health Persp., 79, 43–51, 1989. 13839

Stelson, A. W. and Seinfeld, J. H.: Thermodynamic prediction of the water activity, NH_4NO_3 dissociation constant, density and refractive index for the NH_4NO_3–$(NH_4)_2SO_4$–H_2O system at 25 °C, Atmos. Environ., 16, 2507–2514, 1982. 13831

Stohl, A., Hittenberger, M., and Wotawa, G.: Validation of the Lagrangian particle dispersion model FLEXPART against large-scale tracer experiment data, Atmos. Environ., 32, 4245–4264, 1998. 13842

Stohl, A., Eckhardt, S., Forster, C., James, P., Spichtinger, N., and Seibert, P.: A replacement for simple back trajectory calculations in the interpretation of atmospheric trace substance measurements, Atmos. Environ., 36, 4635–4648, 2002. 13862

Trebs, I., Metzger, S., Meixner, F. X., Helas, G., Hoffer, A., Rudich, Y., Falkovich, A., Moura, M. A. L., da Silva, R. S., Artaxo, P., Slanina, J., and Andreae, M. O.: The NH_4^+–NO_3^-–Cl^-–SO_4^{2-}–H_2O aerosol system and its gas phase precursors at a pasture site in the Amazon Basin: how relevant are mineral cations and soluble organic acids?, J. Geophys. Res.-Atmos., 110, D07303, doi:10.1029/2004JD005478, 2005. 13847

Underwood, G., Song, C., Phadnis, M., Carmichael, G., and Grassian, V.: Heterogeneous reactions of NO_2 and HNO_3 on oxides and mineral dust: a combined laboratory and modeling study, J. Geophys. Res.-Atmos., 106, 18055–18066, 2001. 13831

ACPD
15, 13827–13865, 2015

Usher, C., Michel, A., and Grassian, V.: Reactions on mineral dust, Chem. Rev., 103, 4883–4939, 2003. 13832, 13845

Utsunomiya, S., Jenson, K. A., Keeler, G. J., and Ewing, R. C.: Direct identification of trace metals in fine and ultrafine particles in the Detroit urban atmosphere, Environ. Sci. Technol., 38, 2289–2297, 2004. 13836

Wang, B. and Laskin, A.: Reactions between water-soluble organic acids and nitrates in atmospheric aerosols: recycling of nitric acid and formation of organic salts, J. Geophys. Res.-Atmos., 119, 3335–3351, 2014. 13830

Wexler, A. and Clegg, S.: Atmospheric aerosol models for systems including the ions H^+, NH_4^+, Na^+, SO_4^{2-}, NO_3^-, Cl^-, Br^-, and H_2O, J. Geophys. Res.-Atmos., 7, 4639–4659, 2007. 13838

Yeatman, S., Spokes, L., and Jickells, T.: Comparisons of coarse-mode aerosol nitrate and ammonium at two polluted coastal sites, Atmos. Environ., 35, 1321–1335, 2001. 13831

Young, A. H., Keene, W. C., Pszenny, A. P., Sander, R., Thornton, J. A., Riedel, T. P., and Maben, J. R.: Phase partitioning of soluble trace gases with size-resolved aerosols in near-surface continental air over northern Colorado, USA, during winter, J. Geophys. Res.-Atmos., 118, 9414–9427, 2013. 13838

Zhuang, H., Chan, C. K., Fang, M., and Wexler, A. S.: Formation of nitrate and non-sea-salt sulfate on coarse particles, Atmos. Environ., 33, 4223–4233, 1999. 13831

ACPD
15, 13827–13865, 2015

Table 1. Statistical summary of major gas and particle phase species measured by the MARGA. Concentrations ($\mu g\,m^{-3}$) of each species were collected from 1 June to 13 July 2013 (n = 949) and were averaged over one hour of sample collection.

Species	MDL[a]	Mean ($\pm 1\sigma$ SD)	Minimum	Maximum
HNO_3	0.05	0.34 ± 0.14	[b]	1.14
NH_3	0.05	0.51 ± 0.24	0.15	2.09
SO_2	0.04	0.68 ± 1.47	[b]	16.4
Cl^-	0.02	0.02 ± 0.05	[b]	0.42
NO_3^-	0.04	0.37 ± 0.20	[b]	1.07
SO_4^{2-}	0.03	2.20 ± 1.19	0.50	8.87
NH_4^+	0.03	0.67 ± 0.38	0.11	2.21
Na^+	0.02	0.08 ± 0.09	[b]	0.50
K^+	0.01	0.05 ± 0.06	[b]	0.31
Mg^{2+}	0.01	0.01 ± 0.02	[b]	0.09
Ca^{2+}	0.01	0.05 ± 0.06	[b]	0.31

[a] Minimum Detection Limit (MDL) as reported by Makkonen et al. (2012)
[b] Below Minimum Detection Limit (MDL)

ACPD
15, 13827–13865, 2015

Table 2. Percent composition and element:Si ratios of the two different coarse particle events observed during the summer 2013 SOAS field campaign.

Element	Coarse Particle Event 1 Composition (%)	Coarse Particle Event 1 Si Ratio	Coarse Particle Event 2 Composition (%)	Coarse Particle Event 2 Si Ratio
Al	26.8 %	0.64	26.2 %	0.59
Si	41.8 %	1	45.2 %	1
K	5.1 %	0.12	5.5 %	0.11
Ca	2.4 %	0.06	3.3 %	0.07
Ti	1.1 %	0.03	1.1 %	0.02
Mn	0.2 %	< 0.01	0.1 %	< 0.01
Fe	9.3 %	0.22	9.4 %	0.21
Na	12.0 %	0.31	7.5 %	0.18
Mg	1.4 %	0.02	1.8 %	0.04

Al, Si, K, Ca, Ti, Mn, and Fe data from ARA XRF measurements; Na and Mg from data MARGA measurements; all have 2.5 µm size cut.

ACPD
15, 13827–13865, 2015

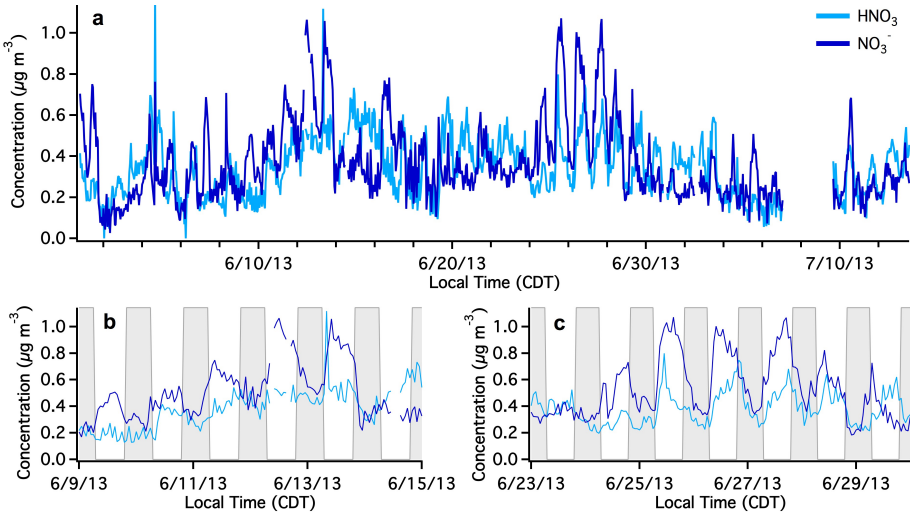

Figure 1. Time series of hourly averaged HNO_3 and NO_3^- concentrations measured by MARGA during the summer SOAS campaign, including the **(a)** full time series and two subsets, with shading indicating nighttime, that encompass the periods of elevated NO_3^- during **(b)** 9 to 15 June and **(c)** 23 to 30 June 2013.

ACPD
15, 13827–13865, 2015

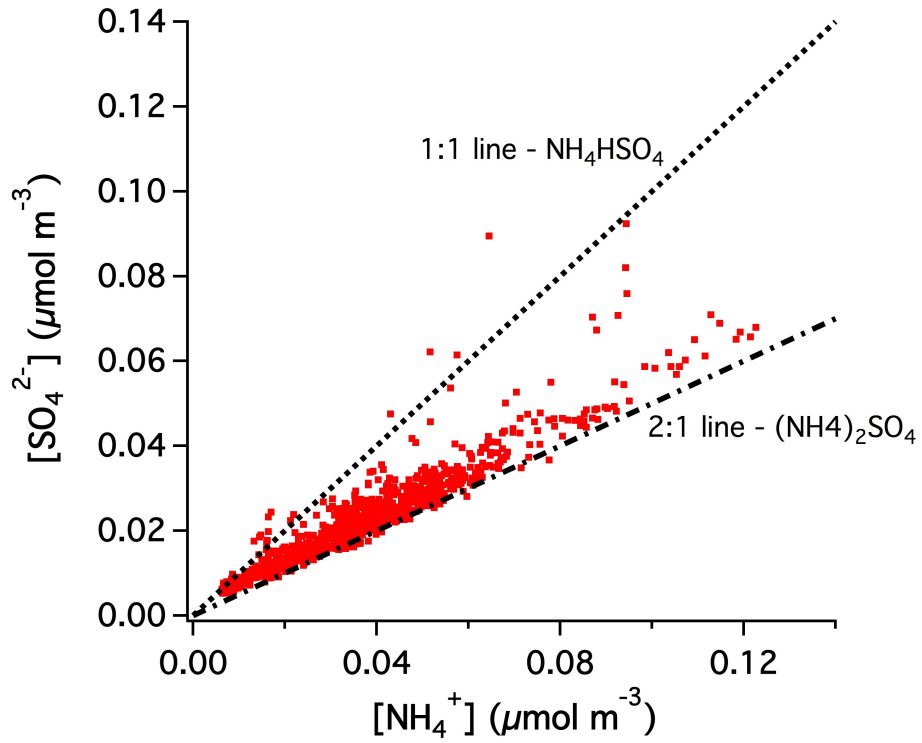

Figure 2. Correlation of SO_4^{2-} and NH_4^+ concentrations measured by MARGA during the 2013 SOAS campaign (1 June to 13 July). The higher concentrations of SO_4^{2-} relative to NH_4^+ show an acidic environment at the SOAS site, with insufficient moles of NH_4^+ present to fully neutralize existing SO_4^{2-} as $(NH_4)_2SO_4$.

ACPD
15, 13827–13865, 2015

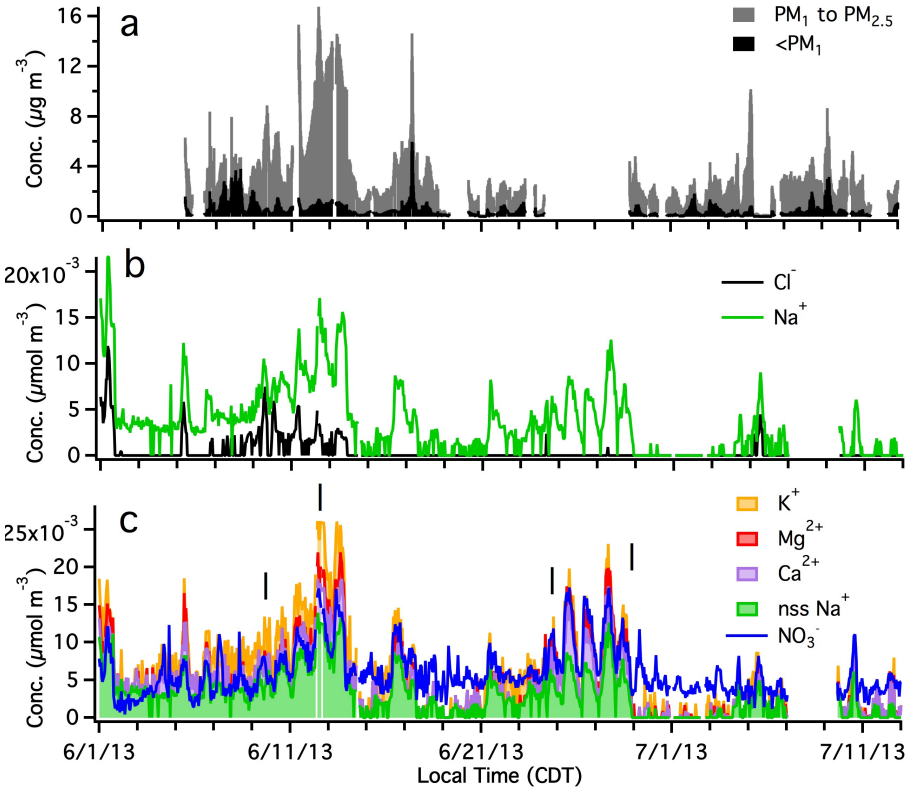

Figure 3. Periods of high aerosol NO_3^- during the SOAS campaign were correlated with **(a)** high PM_1–$PM_{2.5}$ aerosol mass fraction, **(b)** high Na^+ and Cl^- concentrations, indicating the presence of sea spray, and (**c**, stacked) high concentrations of minerals, with molar concentrations sufficient to neutralize measured NO_3^- during coarse mode periods. $Na^+_{residual}$ indicates aerosol Na^+ not associated with Cl^-, calculated by subtracting an equivalent of Cl^- from Na^+. The dates indicated by vertical lines in **(c)** were chosen for wind pattern analysis (Sect. 3.3).

ACPD
15, 13827–13865, 2015

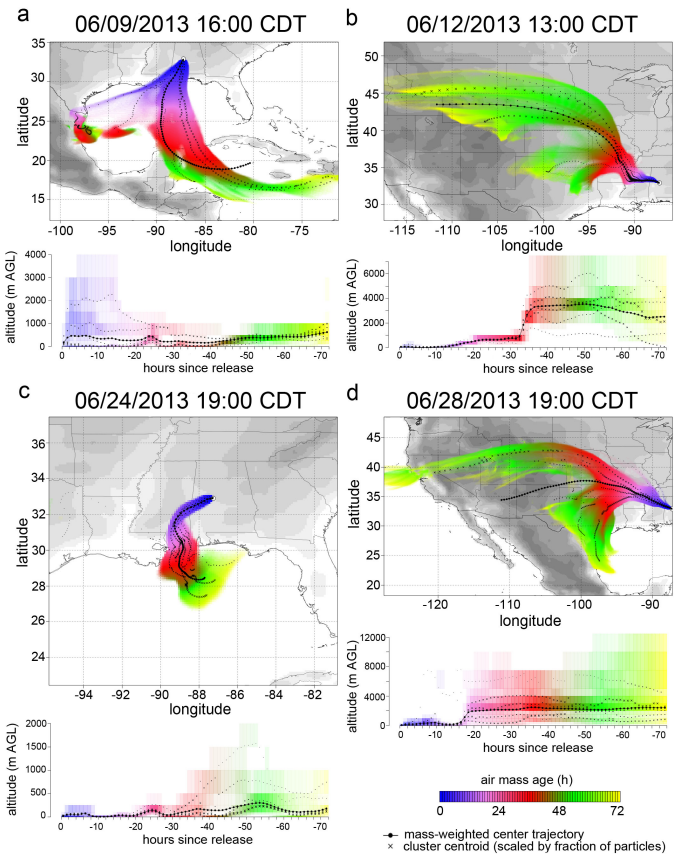

Figure 4. Three-day back trajectories at the Centreville site (circled), showing horizontally integrated (top) and vertically integrated (bottom) trajectories with mass-weighted and cluster centroid trajectories as defined by (Stohl et al., 2002), for **(a)** event 1 on 9 June, **(b)** event 1 on 12 June, **(c)** event 2 on 24 June, and **(d)** event 2 on 28 June. Times shown correlate with peaks indicated by horizontal bars in Fig. 3c.

ACPD
15, 13827–13865, 2015

Inorganic NO_3^- aerosol during the 2013 SOAS campaign

H. M. Allen et al.

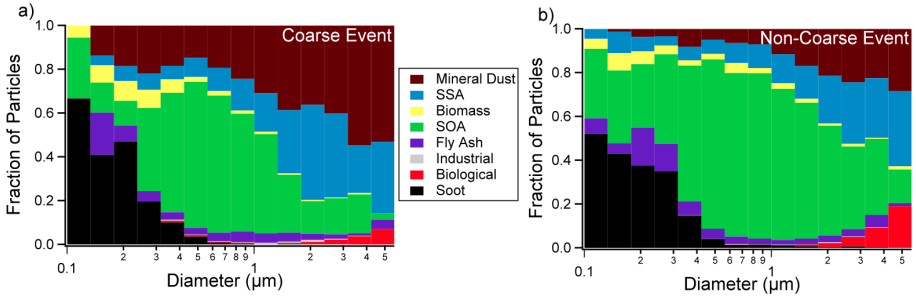

Figure 5. Compositional analysis using SEM with EDX of particles collected during the SOAS campaign as a function of particle diameter during **(a)** the two coarse particle events and **(b)** throughout the remainder of the field campaign. SSA indicates sea spray aerosol and SOA indicates secondary organic aerosol.

ACPD
15, 13827–13865, 2015

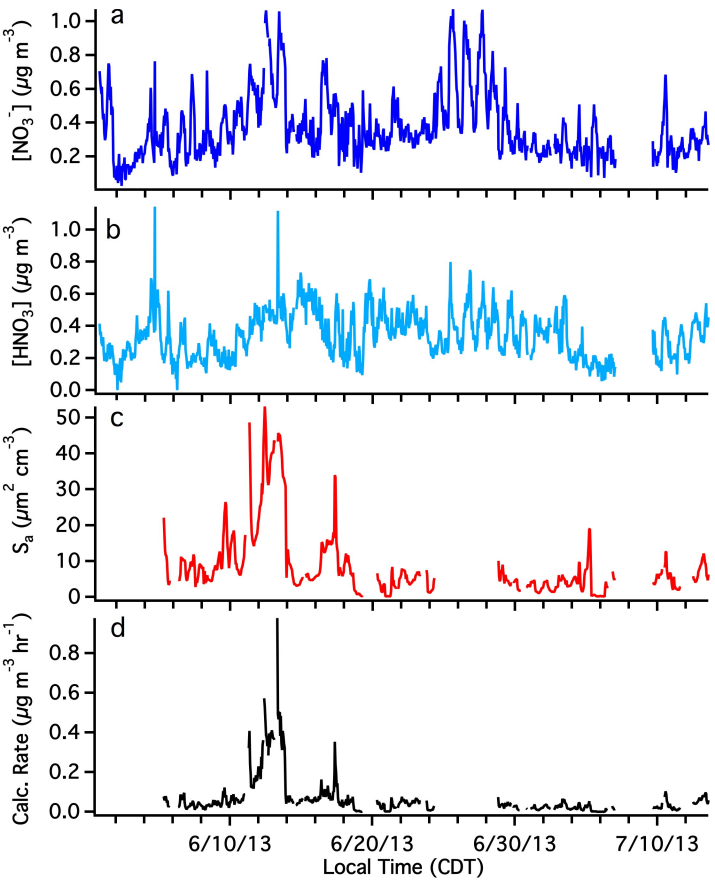

Figure 6. (a) Hourly averaged NO_3^- aerosol concentrations during the 2013 SOAS campaign, compared with factors that contribute to NO_3^- formation such as **(b)** HNO_3 concentrations and **(c)** estimated aerosol surface area of particles with 0.7–2.5 µm diameters. **(d)** The rate of HNO_3 uptake on mineral dust is predominantly driven by $PM_{2.5}$ surface area.

ACPD
15, 13827–13865, 2015

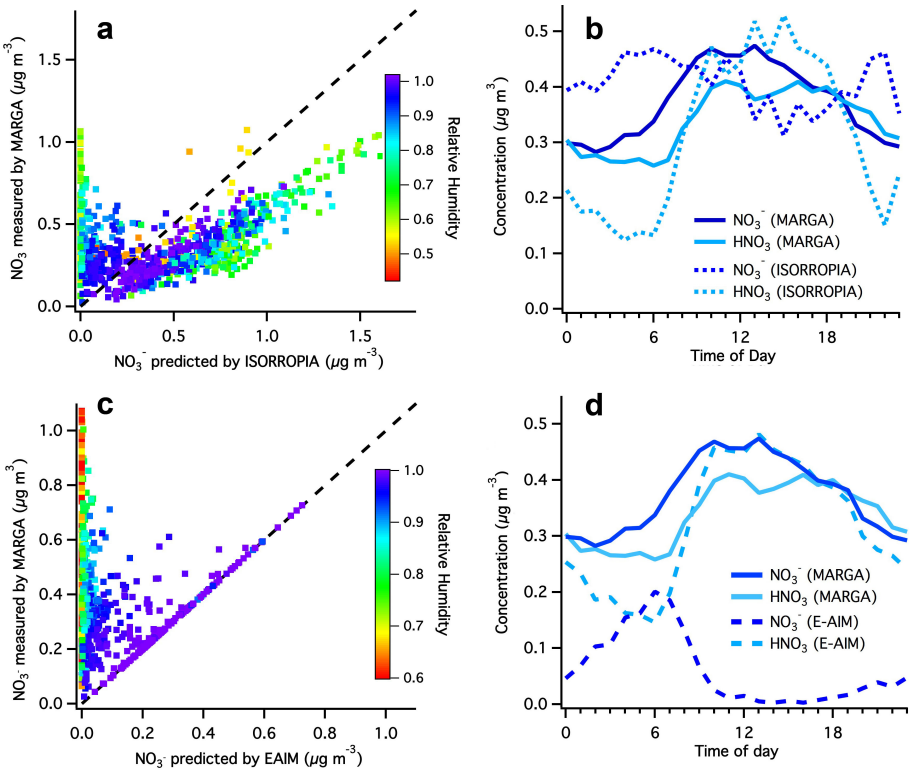

Figure 7. Results of inorganic modeling compared with hourly measurements made by MARGA during the 2013 SOAS campaign. **(a)** Correlation of aerosol NO_3^- between ISORROPIA II and MARGA; **(b)** diurnal pattern of gaseous HNO_3 and aerosol NO_3^- for ISORROPIA II and MARGA; **(c)** correlation of aerosol NO_3^- between E-AIM and MARGA; and **(d)** diurnal pattern of gaseous HNO_3 and aerosol NO_3^- for E-AIM and MARGA.

ACPD
15, 13827–13865, 2015